$\mathscr{L}_1$ Adaptive Control Law in support of Large Flight Envelope Modeling Work

Irene M. Gregory, Enric Xargay, Chengyu Cao, and Naira Hovakimyan

Abstract This paper presents results of a flight test of the $\mathscr{L}_1$ adaptive control architecture designed to directly compensate for significant uncertain cross-coupling in nonlinear systems. The flight test was conducted on the subscale turbine powered Generic Transport Model that is an integral part of the Airborne Subscale Transport Aircraft Research system at the NASA Langley Research Center. The results presented are in support of nonlinear aerodynamic modeling and instrumentation calibration.

1 Introduction

One of the primary objectives of the Integrated Resilient Aircraft Control (IRAC) Project, under the auspices of the NASA Aviation Safety Program, is to advance the state-of-the-art in the adaptive control technology as a means of increasing safety. Of particular interest is piloted flight under adverse conditions such as unusual attitudes, control surface failures, and structural damage. The IRAC Project is using subscale flight testing as an important tool in the evaluation of experimental adaptive

Irene M. Gregory
NASA Langley Research Center, Hampton, VA 23681-2199, USA
Senior Research Engineer, Dynamic Systems and Control, e-mail: irene.m.gregory@nasa.gov

Enric Xargay
University of Illinois at Urbana-Champaign, Urbana, Illinois 61801, USA
Graduate Student, Dept. of Aerospace Engineering, e-mail: xargay@illinois.edu

Chengyu Cao
University of Connecticut, Storrs, CT 06269, USA
Assistant Professor, Dept. of Mechanical Science and Engineering, e-mail: ccao@engr.uconn.edu

Naira Hovakimyan
University of Illinois at Urbana-Champaign, Urbana, Illinois 61801, USA
Professor, Dept. of Mechanical Science and Engineering, e-mail: nhovakim@illinois.edu

control laws. This is particularly beneficial for the test and evaluation of flight control law performance beyond the edge of the normal flight envelope, where the risk of vehicle loss is high due to limited knowledge of nonlinear aerodynamics beyond stall and the potential for high structural loads. The Airborne Subscale Transport Aircraft Research (AirSTAR) facility at the NASA Langley Research Center has been designed to provide a flexible research environment with the ability to conduct rapid prototyping and testing for control algorithms in extremely adverse flight conditions [3, 9, 10].

In addition to testing advanced flight control laws, the AirSTAR has a dual mission of developing aerodynamic models at the edges and beyond the normal flight envelope as well as validating wind tunnel derived models (see Figure 1). This is accomplished through real-time parameter estimation [7, 8], as well as modeling unsteady nonlinear aerodynamics in the (high angle of attack) post-stall region [11, 12]. The parameter estimation work is performed in open loop without any flight control law assisting the pilot, while the nonlinear unsteady aerodynamic modeling requires high precision maneuvers in a highly nonlinear region of the envelope, thus necessitating a command augmentation control law to assist the pilot. Moreover, in order to enable this modeling work, instrumentation must be precisely calibrated all the way to the edges of the controllable flight envelope.

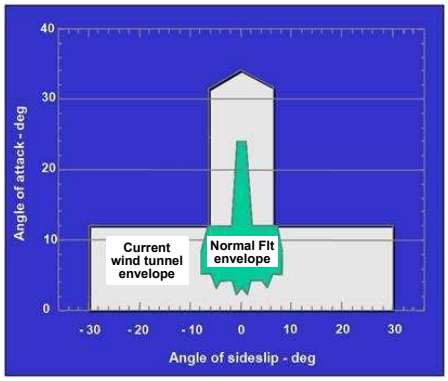

Fig. 1: Extended flight envelope for a typical transport aircraft.

During the September 2010 AirSTAR deployment, an $\mathscr{L}_1$ adaptive flight control law was used to facilitate angle of attack and angle of sideslip vane calibration, which required precise tracking with reduced pilot workload. This paper presents flight test results of the angle of attack and angle of sideslip vane calibration that illustrate the performance of an $\mathscr{L}_1$ controller in support of these calibration tasks. In fact, the results in this paper provide a good demonstration of the tracking precision achieved by the flight control law to the very edge of the controllable envelope.

The rest of the paper is organized as follows. A brief overview of the AirSTAR flight test vehicle is provided in Section 2. Section 3 presents a short description of

Fig. 2: AirSTAR flight test aircraft.

the $\mathscr{L}_1$ flight control law used in the September 2010 flight tests. Section 4 describes the flight test results. Finally, Section 5 presents concluding remarks.

2 AirSTAR Infrastructure

Currently, AirSTAR's primary test aircraft is a 5.5% dynamically scaled twin-turbine powered generic transport model (GTM) shown in Figure 2. Dynamic scaling (i.e., similitude using equal Froude number and relative density between model-scale and full-scale) allows subscale flight test results to be applied to full-scale aircraft. This vehicle (GTM tail number T2) has a 6.5 ft wingspan, weighs 54 lbs at takeoff, and has a flight time of approximately 20 minutes. The aircraft is outfitted with full flight-test instrumentation, including angle of attack and angle of sideslip vanes, sensors measuring static and dynamic pressure, control surface position sensors, rate gyros and accelerometers, a 6-DOF INS/GPS package, and engine instrumentation. Downlink data update rates vary from 5 Hz on the GPS data to 200 Hz on the data from analog sensors. Uplink commands are transmitted at 200 Hz.

The GTM aircraft has been extensively tested in NASA Langley wind tunnels with particular emphasis on modeling nonlinear regions of the extended flight envelope well beyond nominal flight. The high-fidelity nonlinear simulation of the GTM aircraft, built up from the extensive wind tunnel data, has been updated with the data obtained during the September 2009 flight test and validated with subsequent flight tests in 2010. The concept of operations, details of the facility and operational software can be found in [3, 9, 10].

3 $\mathscr{L}_1$ Flight Control Law

The research control law developed for the GTM aircraft has as its primary objective achieving tracking for a variety of tasks with guaranteed stability and robustness in the presence of uncertain dynamics, such as changes due to rapidly varying flight conditions during standard maneuvers, and unexpected failures. Ideally, all of these tasks must be achieved while providing Level I handling qualities under nominal as well as adverse flight conditions. The $\mathscr{L}_1$ flight control law used in the September 2010 deployment consists of a nonadaptive stability augmentation system (SAS) and a three axes angle of attack (α), roll rate (p)–sideslip angle (β) command augmentation system (CAS), which is based on the theory presented in [13]. The α command was chosen to facilitate modeling which requires precise AOA tracking, while the p–β command is one of the standard lateral-directional response types. The $\mathscr{L}_1$ control law with its main elements is represented in Figure 3.

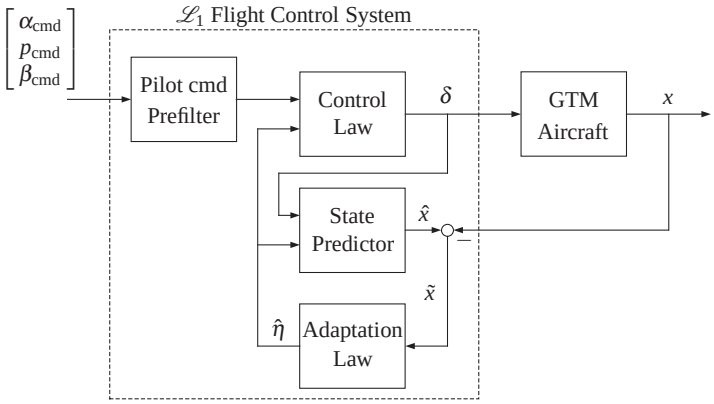

Fig. 3: Block diagram of the $\mathscr{L}_1$ flight control architecture. The $\mathscr{L}_1$ control law consists of a fast estimation scheme and a control law. The fast estimation scheme includes a state predictor and an adaptation law, which are used to generate estimates $\hat{\eta}$ of the plant uncertainties. The state predictor generates a prediction $\hat{x}$ of the system state that, when subtracted from the actual system state x, yields an error signal $\tilde{x}$ that drives the adaptation process. The adaptation law updates the estimates of the plant uncertainties at a high adaptation rate. Based on the uncertainty estimates, the control law generates control surface deflection commands δ as the output of lowpass filters.

The design of an $\mathscr{L}_1$ adaptive flight control law for the GTM is based on the linearized dynamics of the aircraft at a nominal flight condition corresponding to an equivalent airspeed of 80 knots and an altitude of 1000 ft. These linear dynamics are further simplified to include only short-period dynamics in the longitudinal axis and

roll rate, angle of sideslip, and yaw rate in the lateral-directional dynamics, neglecting bank angle ϕ. Since the airplane is Level I at this flight condition, the nominal desired dynamics of the linear state predictor are chosen to be similar to those of the airplane. However, additional damping is added to the longitudinal and directional dynamics of the state predictor, while the lateral dynamics of the predictor are set to be slightly faster than the lateral dynamics of the aircraft in order to satisfy performance specifications. The state predictor of the $\mathscr{L}_1$ controller is scheduled to specify different performance requirements at special flight regimes such as high speed above the allowable research envelope and post-stall high angle of attack. In order to improve the handling qualities of the airplane, a linear prefilter is added to the adaptive flight control law so as to ensure desired decoupling properties as well as desired command tracking performance. Overdamped second-order lowpass filters with unity dc gain are used in all control channels, while their bandwidths are set to ensure minimum total time delay margin of 0.125 s and a gain margin of 6 dB. Finally, the adaptation sampling time is set to $T_s = \frac{1}{600}$ s, which corresponds to the execution speed of the AirSTAR flight control computer. Note that the same control parameters for the prefilter, the lowpass filters, and the adaptation rate are used across the entire flight envelope with no scheduling or reconfiguration. Further background, details about the design, and previous piloted simulation evaluations and flight tests of the $\mathscr{L}_1$ adaptive flight control law can be found in [4, 5].

4 Flight Test Results

On the third deployment, the $\mathscr{L}_1$ adaptive flight control law has established itself as a reliable and predictable tool to be used in support of other research tasks in order to reduce research pilot's workload and provide tighter acquisition of target flight conditions. One of these research tasks flown during the September 2010 deployment was the calibration of the two air-data vanes placed on each wingtip of the GTM aircraft (see Figure 2). The angle of attack and the angle of sideslip measurements obtained from the vanes are used in both modeling and control. The flight test was conducted in strict adherence to the procedures outlined in the flight test plan [2] and the test cards [1], relevant sections of which are summarized here to provide the necessary background to put the presented results in the appropriate context.

Standard methods for angle of attack and the angle of sideslip vane calibration can be found in [6]. The calibration algorithm requires accurate tracking of commanded angle of attack and angle of sideslip. The particular methodology evaluated with the following tasks is executed in near real time and utilizes real-time parameter estimates. The $\mathscr{L}_1$ adaptive flight control law was employed to provide precision tracking of commanded variables, keep other aircraft states within tight limits, and reduce pilot's workload. For the angle of attack vane calibration, various thrust levels were specified in terms of percent RPM and were set at the beginning of the maneuver. This provided variation in angle of attack rate of change and ultimately affected the range calibrated. This set of maneuvers for angle of attack vane cali-

bration was flown manually by the research pilot. On the other hand, the angle of sideslip vane calibration maneuvers involved flat turns with a sideslip angle ramp command to various steady-state values which were then held until the range boundary was approached. The sideslip angle command was a generated wave train, while the pilot was responsible for flying the other axes.

4.1 Angle of Attack Vane Calibration

The angle of attack calibration was approached with two different strategies. The first strategy was setting a specific throttle RPM such that the angle of attack climbed steadily until the test range boundary was approached. The throttle setting and the subsequent angle of attack response are illustrated in Figures 4a and 4b. Note that the angle of attack reaches stall and slightly above, 13 deg $< \alpha <$ 14 deg. For the GTM T2 aircraft, stall has been determined to occur around $\alpha = 12$ deg. This region is characterized by rapidly changing roll damping that varies from stable to slightly unstable in the 10 to 12 deg range and an unstable pitch break that occurs at 13 deg angle of attack. This maneuver is repeated twice, from about 872 to 892 seconds, followed by recovery, turn and repeat of the maneuver from 920 to 940 seconds. From Figure 4c note that there is a steady longitudinal stick pull and concurrently a steady and small lateral stick implying minimal roll dynamics (Figure 4c, between around 870 and 890 s, and 925 and 940 s). The second strategy was based in selecting a throttle setting that corresponded to a specific constant angle of attack. The constant angles of attack were $\alpha = 5, 8, 10, 12$ deg as illustrated in Figure 5. The precision of the angle of attack tracking even in the stall and near stall region is illustrated in Figures 6a and 7a. The $\mathscr{L}_1$ adaptive flight control law is taking care of the rapid change of the roll dynamics in this angle of attack region, $\alpha = 10, 12$ deg, as can be observed from essentially neutral lateral stick and zero roll rate during angle of attack tracking (Figures 6b-6c and 7b-7c).

4.2 Angle of Sideslip Vane Calibration

The angle of sideslip vane calibration involved flat turn maneuvers with angle of sideslip ramp command for various steady-state values, with a maximum of $|\beta| =$ 8 deg dictated by maximum aileron deflection to counteract roll rate and maintain a flat turn. The sideslip angle command was ramped up at 2 $\frac{\text{deg}}{\text{s}}$ and at 1 $\frac{\text{deg}}{\text{s}}$ and then held for $\beta = \pm 2, \pm 4, \pm 6, \pm 8$. This set of maneuvers required tight tracking of the sideslip angle command and minimal roll dynamics (desired bank angle is less than $\pm$2 deg, adequate less than $\pm$4 deg). The sideslip angle command is provided by an automated wave-train while the pilot flies the roll and pitch axes. An entire flight was dedicated to sideslip angle vane calibration and the task is illustrated in

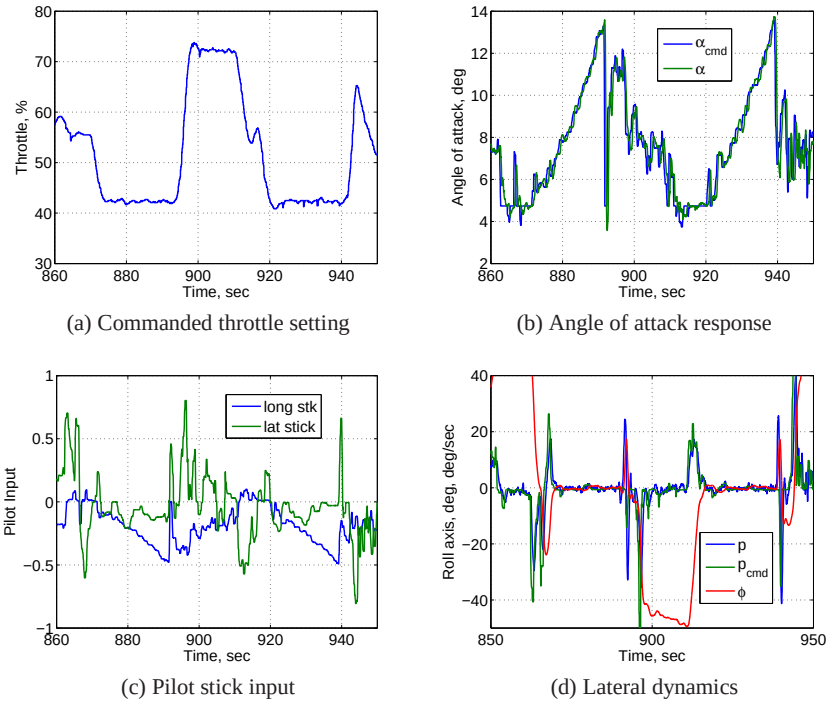

(a) Commanded throttle setting (b) Angle of attack response

(c) Pilot stick input (d) Lateral dynamics

Fig. 4: Variable α strategy

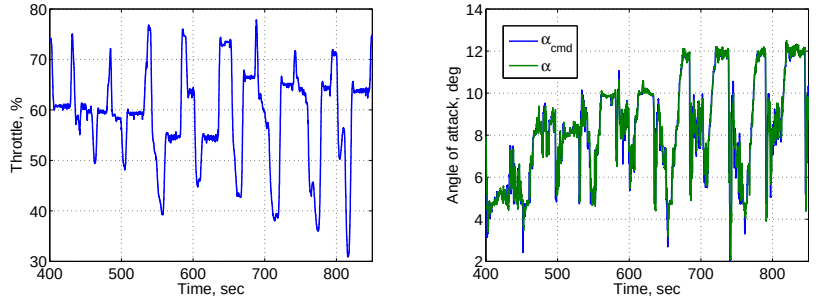

(a) Commanded throttle setting (b) Angle of attack response

Fig. 5: Constant α strategy

Figure 8. Note that each value for commanded angle of slideslip was flown twice, on the up wind and down wind legs of the circuit.

Precision tracking of the more extreme cases and the associated dynamics are shown in Figures 9 and 10. Commanded sideslip of $+8$ deg and corrective pilot stick inputs to maintain the flat turn are shown in Figure 9. Examining the sideslip angle

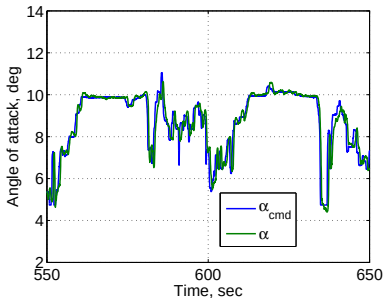

(a) Angle of attack

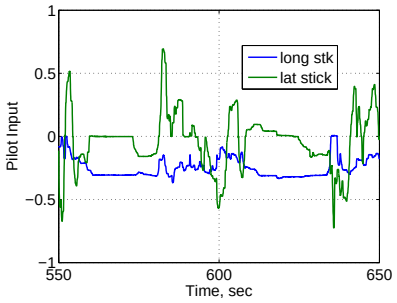

(b) Pilot stick input

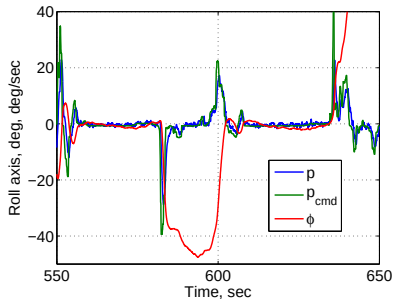

(c) Lateral dynamics

Fig. 6: Constant α strategy: 10 deg angle of attack acquisition

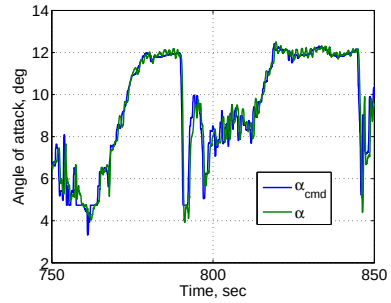

(a) Angle of attack

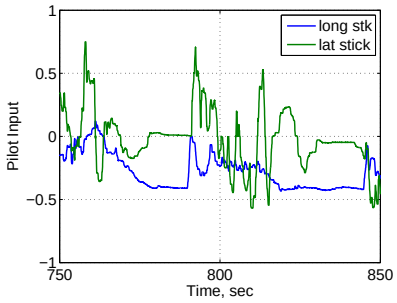

(b) Pilot stick input

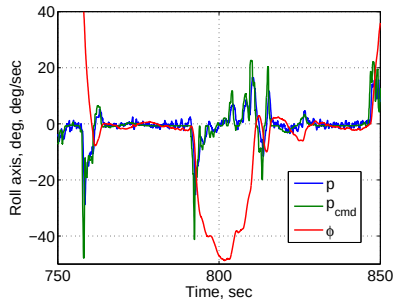

(c) Lateral dynamics

Fig. 7: Constant α strategy: 12 deg angle of attack acquisition

response in Figure 9a and the actuator responses in Figures 9e and 9f, it becomes evident that the airplane is unable to hold a flat turn of $\beta = +8$ deg. Initially, the pilot commands lateral stick to counteract roll induced by the flat turn. However, the ailerons are not sufficient to cancel the induced roll rate; in fact, Figure 9e illustrates that the ailerons are saturated during the flat turn maneuvers at $\beta = +8$ deg, with an aileron command that significantly exceeds the deflection limit. The inability to

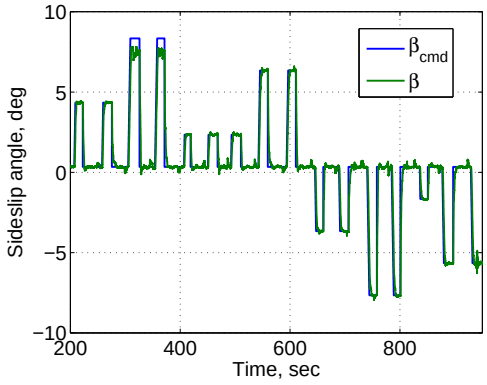

Fig. 8: Angle of sideslip vane calibration task.

counteract the induced roll rate at $\beta = +8$ deg results in the pilot holding a nonzero lateral stick command during the flat turn maneuvers (Figure 9b). This lateral stick is translated into a nonzero roll rate command (Figure 9c), which in turn reduces the rudder deflection as the control law uses both aileron and rudder to achieve the commanded roll rate. At this point, the pilot's adjustment of lateral stick results in rudder deflection such that the roll rate of the aircraft is canceled. In fact, in Figures 9f and 9a, one can see that the wiggles in the lateral stick commanded by the pilot lead to small wiggles in the rudder deflection command, and also manifest themselves as wiggles in the sideslip angle response. As a result, the pilot ends up performing a stable flat turn at approximately $\beta = +7.5$ deg, while holding the roll rate within the ± 10 deg range (Figure 9c), and keeping –with a couple of minor exceptions at 315 s and 361 s– the bank angle within adequate range for both legs of the maneuver (Figure 9d). Note that the aircraft is executing a turn between 330 and 345 s.

The behavior of the aircraft for the flat turn at $\beta = -8$ deg is shown in Figure 10. In this case, the pilot is able to maintain the flat turn at the desired angle of sideslip. The pilot stick inputs to maintain flat turn are plotted in Figure 10b and the corresponding roll-rate response is shown in Figure 10c. In this case the pilot initiates a reasonably steady lateral stick offset to counter the flat turn induced roll and makes only minor tweaks during $\beta = -8$ deg. This stick behavior translates into actual roll rate close to measurement noise levels and the bank angle remaining within adequate range during sideslip angle buildup and in desired range during sideslip angle hold as seen from Figure 10d. The actuator responses are shown in Figures 10e and 10f with ailerons once again saturated for the duration of constant sideslip angle hold time. The reason for this asymmetric response to $|\beta| = 8$ deg is still under investigation; however, the conjecture is aircraft asymmetry and/or patch of turbulence. Recall that the maximum sideslip angle command magnitude was determined to correspond to the maximum roll controllability by the ailerons in the AirSTAR simulation.

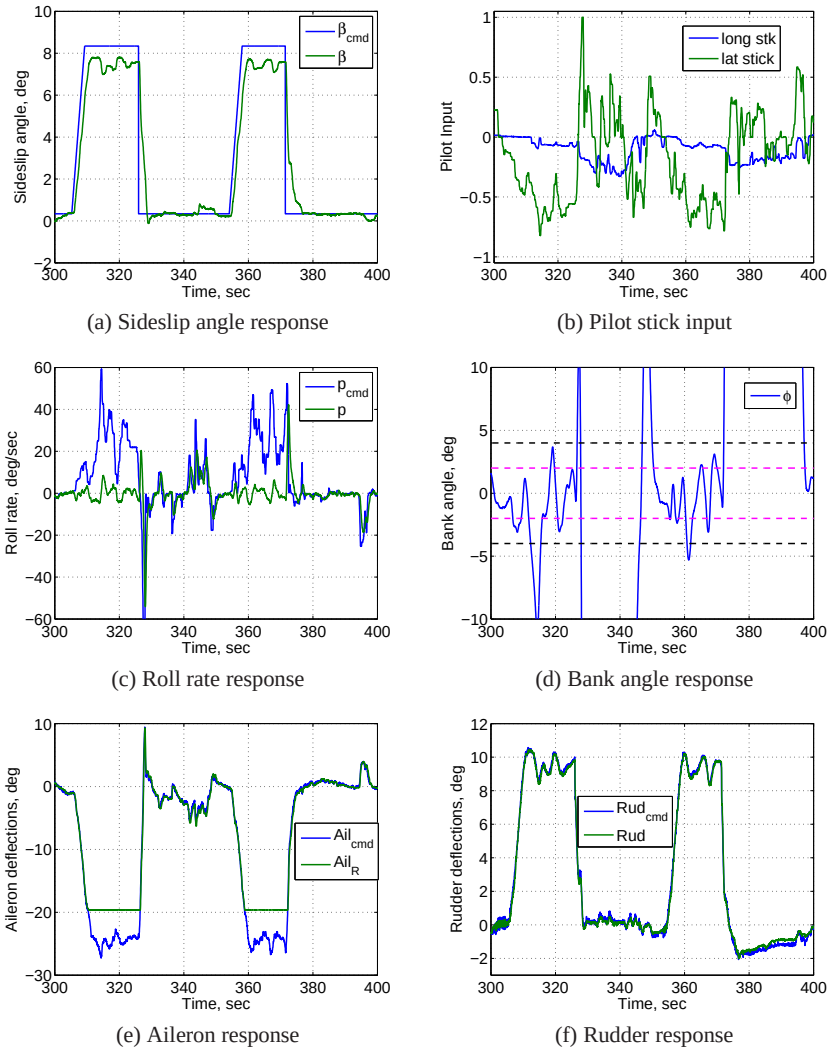

(a) Sideslip angle response

(b) Pilot stick input

(c) Roll rate response

(d) Bank angle response

(e) Aileron response

(f) Rudder response

Fig. 9: Angle of sideslip vane calibration. Command $+8$ deg.

These flight tests unexpectedly illustrate the ability of the MIMO $\mathscr{L}_1$ flight control law to maintain a stable flat turn even if the commanded angle of sideslip is beyond achievable value. If the controller architecture had decoupled the roll rate and the rudder, the aircraft would have rolled off as an angle of sideslip of $+8$ deg was commanded. This is another demonstration of the graceful degradation of performance provided by the $\mathscr{L}_1$ adaptive control law when nominal performance is not achievable. Moreover, note that the $\mathscr{L}_1$ control law remains stable and predictable even when the ailerons are completely saturated.

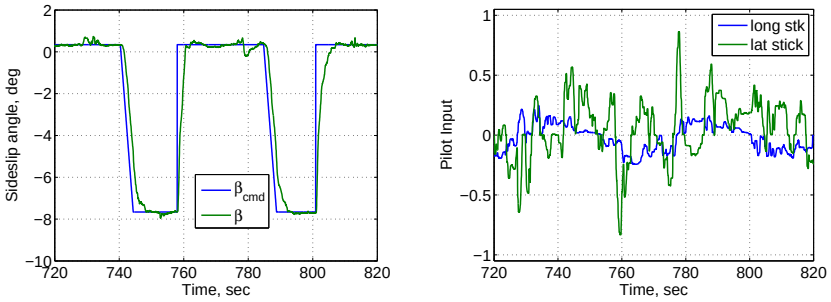

(a) Sideslip angle response

(b) Pilot stick input

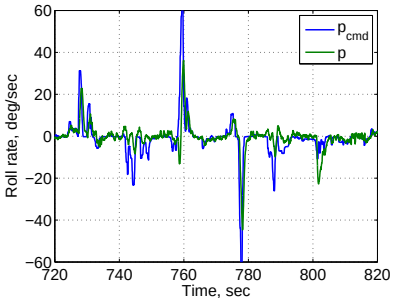

(c) Roll rate response

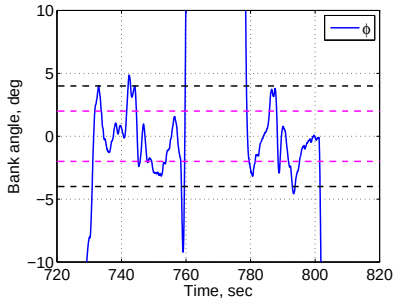

(d) Bank angle response

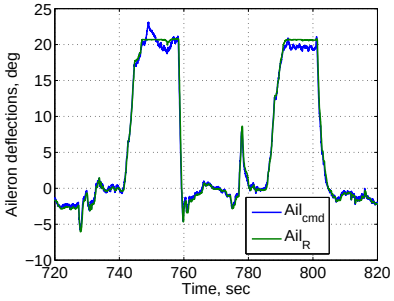

(e) Aileron response

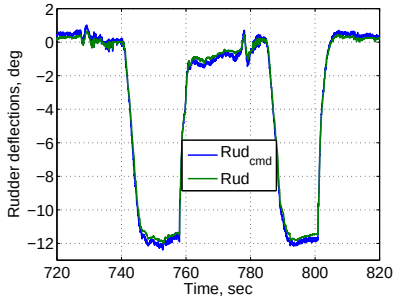

(f) Rudder response

Fig. 10: Angle of sideslip vane calibration. Command -8 deg.

5 Conclusions

The results presented in this paper illustrate the use of an $\mathscr{L}_1$ flight control law in support of utilizing the AirSTAR aircraft as a flying wind tunnel by providing tighter acquisition of target flight conditions. The control law demonstrates precision tracking capability across the flight envelope, and a graceful performance degradation when the target flight conditions are beyond achievable values and the control sur-

faces are persistently saturated. Moreover, the $\mathscr{L}_1$ control law provides predictable response to the pilot when the control authority for different axes is divided between a pilot and an automatic command. The ability of the $\mathscr{L}_1$ control law to deal with both matched and unmatched uncertainties in addition to fast adaptation is what allows a controller with very limited gain scheduling to cover a large flight envelope.

Acknowledgments

The authors would like to acknowledge the staff of the AirSTAR Flight Test Facility for their support with control law implementation and piloted evaluations.

References

[1] Cunningham K (2010) AirSTAR Flight Test Cards v3.12. Technical Report GTMP–6325 2010.03, NASA Langley Research Center
[2] Cunningham K (2010) AirSTAR Flight Test Plan: 5.5% dynamically scaled GTM tail number T2. Deplyoment 2010.03. Technical Report GTMP–6326 2010.03, V 1.00, NASA Langley Research Center
[3] Cunningham K, Foster JV, Morelli EA, Murch AM (2008) Practical application of a subscale transport aircraft for flight research in control upset and failure conditions. In: AIAA Atmospheric Flight Mechanics Conference, Honolulu, HI, AIAA-2008-6200
[4] Gregory IM, Cao C, Xargay E, Hovakimyan N, Zou X (2009) $\mathscr{L}_1$ adaptive control design for NASA AirSTAR flight test vehicle. In: AIAA Guidance, Navigation and Control Conference, Chicago, IL, AIAA-2009-5738
[5] Gregory IM, Xargay E, Cao C, Hovakimyan N (2010) Flight test of an $\mathscr{L}_1$ adaptive controller on the NASA AirSTAR flight test vehicle. In: AIAA Guidance, Navigation and Control Conference, Toronto, Canada, AIAA-2010-8015
[6] Lawford JA, Nippress KR (1983) AGARD flight test techniques series. Volume 1 on Calibration or air-data systems and flow direction sensors. Technical Note AGARD-AG-300-VOL.I, (NATO) Advisory Group for Aerospace Research and Development
[7] Morelli EA (2010) Real-time aerodynamic parameter estimation without air flow angle measurements. In: AIAA Atmospheric Flight Mechanics Conference, Toronto, Canada, AIAA-2010-7951
[8] Morelli EA, Smith MS (2009) Real-time dynamic modeling: Data information requirements and flight-test results. Journal of Aircraft 46(6):1894–1905
[9] Murch AM (2008) A flight control system architecture for the NASA AirSTAR flight test infrastructure. In: AIAA Guidance, Navigation and Control Conference, Honolulu, HI, AIAA-2008-6990
[10] Murch AM, Cox DE, Cunningham K (2009) Software considerations for subscale flight testing of experimental control laws. In: AIAA Infotech@Aerospace Conference and AIAA Unmanned... Unlimited Conference, Seattle, WA, AIAA-2009-2054
[11] Murphy PC, Klein V (2008) Transport aircraft system identification from wind tunnel data. In: AIAA Atmospheric Flight Mechanics Conference, Honolulu, HI, AIAA-2008-6202
[12] Murphy PC, Klein V (2010) Transport aircraft system identification using roll and yaw oscillatory wind tunnel data. In: AIAA Atmospheric Flight Mechanics Conference, Toronto, Canada, AIAA-2010-8122
[13] Xargay E, Hovakimyan N, Cao C (2010) $\mathscr{L}_1$ adaptive controller for multi-input multi-output systems in the presence of nonlinear unmatched uncertainties. In: American Control Conference, Baltimore, MD